



# Fabrication of single-crystal silicon micro pillars on copper foils by nanosecond pulsed laser irradiation

Jiwang Yan (2)<sup>a,\*</sup>, Jun Noguchi<sup>a</sup>, Yoshitake Terashi<sup>b</sup>

<sup>a</sup> Department of Mechanical Engineering, Keio University, Hiyoshi 3-14-1, Kohoku-ku, Yokohama 223-8522, Japan

<sup>b</sup> Central Research Institute, Kyocera Corporation, Hebimizō-cho 1166-6, Higashiōmi, Shiga 527-8555, Japan



## ARTICLE INFO

### Article history:

Available online 29 April 2017

### Keywords:

Selective laser melting  
Silicon  
Micro structure

## ABSTRACT

A nanosecond pulsed Nd:YAG laser was used to irradiate a mixture of silicon powders, polyimide and carbon black deposited onto a copper foil. Silicon micro pillars with a single-crystalline structure were successfully created through laser-induced material self-organization. The shape, orientation and growth rate of the pillars were controllable by varying the fluence, incident angle and scan speed of the laser. The resulting pillar-on-foil structures were applied as negative electrodes of lithium ion batteries, and excellent electrical capacities as well as charge/discharge cycle characteristics could be obtained. The applicability of the proposed method to the manufacture of three-dimensional microstructures was demonstrated.

© 2017 Published by Elsevier Ltd on behalf of CIRP.

## 1. Introduction

Silicon (Si) micro pillars are important surface structures having unique properties, such as antireflective ability and controllable wettability, and thus are interesting for applications in many fields, e.g., for energy harvesting, super hydrophobicity, biomolecule analysis, and so on [1–3]. Currently, Si micro pillars are fabricated on Si wafers by chemical etching or reactive-ion etching [4]. However, there is minimal literature on fabricating Si micro pillars on metal substrates, even though they have a wide range of potential applications. Like Si-based porous nanocomposites [5–8], Si micro pillars on metal foils are expected as new materials for fabricating lithium ion battery electrodes, which have a theoretical capacity ten times higher than that of a conventional carbon electrode.

In this study, a novel method for fabricating Si micro pillars on a copper (Cu) foil was developed based on nanosecond pulsed laser irradiation of a mixture of Si powders, polyimide (as a binder), and carbon black (as a sacrificial agent) deposited on the Cu foil. The shape, orientation, crystallinity and growth rate of the pillars were investigated under various conditions. The performance of the fabricated pillar-on-foil structure as an electrode for a lithium ion battery was evaluated and the results thereof strongly demonstrate the effectiveness of the proposed method.

## 2. Mechanism for laser-induced pillar formation

Si pillars were fabricated through an additive manufacturing approach [9–11] by laser-induced material self-organization. As illustrated in Fig. 1, Si grains at the top layer are directly heated by

the laser and melt (a–b). The melted Si descends/flows to cover Si grains at the lower layer. With further laser heating, the lower Si grains are also melted due to thermal conduction from the upper layer (c). After Si has been completely melted, it spreads and wets the Cu foil (c). Due to surface tension, liquid Si grains merge to form big Si islands on the Cu foil (e). Under laser irradiation, carbon black, which is used as a sacrificial agent, undergoes plasma gasification and partial ignition in air, generating a high-pressure plasma and carbon oxide gas around the liquid Si islands (f). Due to the plasma-induced pressure, the liquid Si islands are stretched along the laser beam direction, forming long and thin micro pillars after resolidification (g). The polyimide binder has a very high thermal stability, and thus is less influenced by laser irradiation. It remains at the pillar/foil boundary through solid state and/or partial melt bonding [12], and strengthens the Si/Cu interface. This pillar fabrication method has never been reported before.

As shown in Fig. 2(a), when Si bulk is used as a lithium ion battery electrode, ion storage causes Si to expand by a factor of three to four, which causes fracture of the electrode. In contrast, Si pillars can accommodate the volume expansion due to the available space around the pillars, as shown in Fig. 2(b). As a

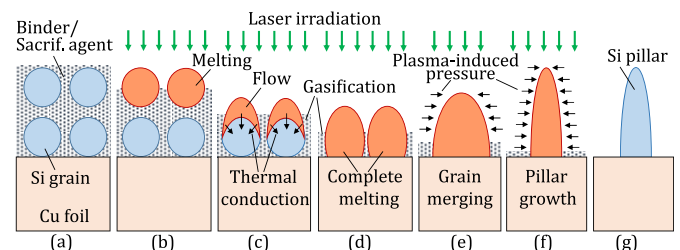


Fig. 1. Model for laser-induced micro pillar formation.

\* Corresponding author.

E-mail address: [yan@mech.keio.ac.jp](mailto:yan@mech.keio.ac.jp) (J. Yan).

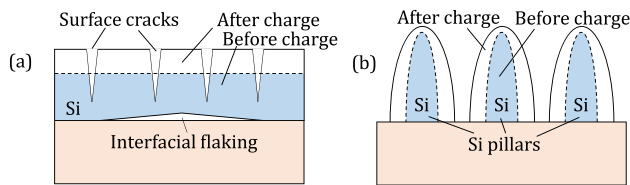


Fig. 2. Model of charge-induced expansion for (a) bulk Si and (b) Si pillars.

consequence, the pillar-on-foil structure may be a breakthrough in the fabrication of Si-based lithium ion batteries.

### 3. Experimental procedures

Laser irradiation experiments were carried out using a Nd:YAG laser with a wavelength of 532 nm. At this wavelength, the laser light can penetrate into Si up to a depth of  $\sim 1 \mu\text{m}$ , which matched the average grain size of the Si powders. The laser pulse duration was 48.4 ns. The laser beam had a Gaussian profile with a diameter of  $85 \mu\text{m}$ . The laser fluence was changed in a range of 529–2643  $\text{mJ}/\text{cm}^2$ , while the scan speed was varied from 1 to 10  $\text{mm}/\text{s}$ . The laser beam was scanned over an area of  $300 \times 300 \text{mm}^2$  by a galvanometer mirror. The workpiece was placed on a stage, which was adjustable in vertical direction to change the focus position of the laser beam.

A mixture of Si powders, polyimide, and carbon black was used as a specimen. Rather than using expensive pure Si nanoparticles, we used waste Si powder from a wire saw slicing process for Si wafers in the manufacturing of solar cells [6,7]. The Si grains (melting point  $1414^\circ\text{C}$ ) ranged in size from a few sub-microns to several microns. Carbon black (ignition point  $520^\circ\text{C}$ ), which contained carbon nanoparticles with sizes ranging from a few nanometer to hundreds of nanometer, was used as a sacrificial agent. Polyimide, which is an infusible polymer of imide monomers, was used as an interfacial binder. The carbon black and the polyimide were added into the Si powders at a mass ratio of 10:15:75. The mixture was agitated by a ball mill to obtain a slurry into which *N*-methylpyrrolidone was added as an organic solvent. Then, a 10–200  $\mu\text{m}$  thick layer of the slurry was deposited onto the Cu foil and dried at  $100^\circ\text{C}$ . The Cu foil thickness was  $50 \mu\text{m}$ . The laser irradiation experiments were conducted in air.

### 4. Results and discussion

#### 4.1. Effect of laser fluence and scan speed

Fig. 3 displays scanning electron microscopy (SEM) images of an irradiated mixture of Si, polyimide and carbon black at various laser

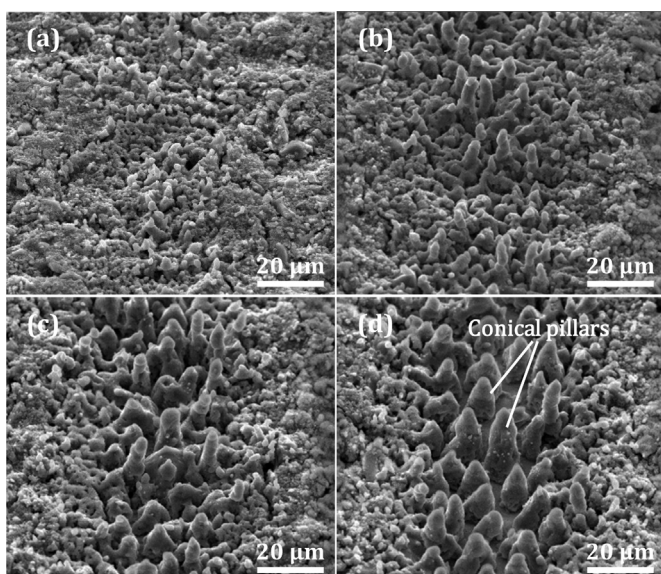


Fig. 3. Micro pillar growth at various laser fluences: (a) 529, (b) 1057, (c) 1586, (d) 2115  $\text{mJ}/\text{cm}^2$ , and a scan speed of 10  $\text{mm}/\text{s}$ .

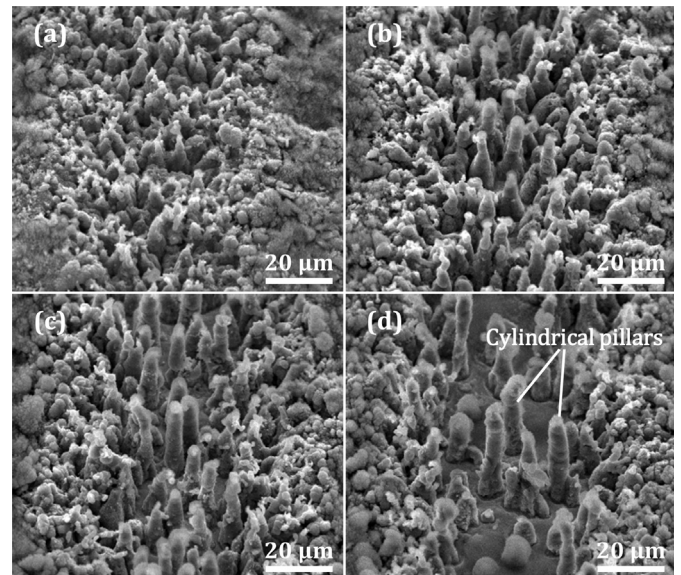


Fig. 4. Micro pillar growth at various laser fluences: (a) 529, (b) 1057, (c) 1586, and (d) 2115  $\text{mJ}/\text{cm}^2$  and a scan speed of 1  $\text{mm}/\text{s}$ .

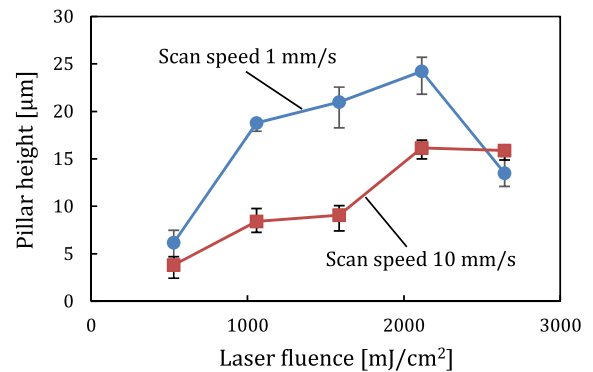


Fig. 5. Change of pillar height with laser fluence and scan speed.

fluences (slurry thickness  $10 \mu\text{m}$ , laser scan speed 10  $\text{mm}/\text{s}$ ). As the laser fluence increased, micro pillars appeared and grew continuously in height. At a laser fluence of 2115  $\text{mJ}/\text{cm}^2$ , individual conical micro pillars were formed with a height of  $\sim 15 \mu\text{m}$ , as shown in Fig. 3(d). Fig. 4 displays SEM images of irradiated samples at a laser scan speed of 1  $\text{mm}/\text{s}$ , i.e., lower than that for the samples shown in Fig. 3. As laser fluence increased, micro pillars grew faster and were thinner than those shown in Fig. 3. At a laser fluence of 2115  $\text{mJ}/\text{cm}^2$  (Fig. 4(d)), nearly cylindrical micro pillars were formed. The height of the tallest one was over  $25 \mu\text{m}$ . In this case, the formation of micro pillars looked similar to the formation of Si micro wires observed in infrared light sintering of Si-based composites [7], indicating the possibility of a vapor-phase pillar growth, i.e., Si is partially evaporated and deposited on the top of the pillars.

Fig. 5 is a plot of the change of pillar height with laser fluence and scan speed. In the figure, the pillar height is defined as the average height of all identifiable pillars over a laser scan distance of  $500 \mu\text{m}$ . As a general trend, pillar height increased with laser fluence, but decreased with laser scan speed. It should be noted that, at a very high laser fluence ( $2643 \text{mJ}/\text{cm}^2$ ) and a low scan speed (1  $\text{mm}/\text{s}$ ), the number of pillars was reduced due to successive laser irradiation, leading to a sharp drop in the curve.

#### 4.2. Effect of laser incident angle

To investigate the relationship between pillar growth and the incident direction of the laser, experiments were conducted at various laser incident angles. Fig. 6 shows SEM photographs of micro pillars formed at a laser incident angle of  $60^\circ$  for various laser fluences. It is clear that the pillars are orientated at an angle of  $\sim 60^\circ$  away from the vertical direction. This observation indicates

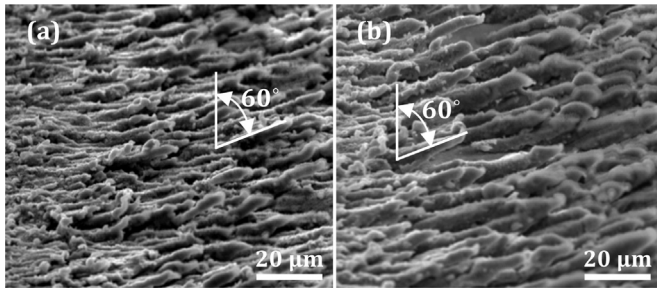


**Fig. 6.** Micro pillars formed at a laser incident angle of 60° and various laser fluences: (a) 1353, (b) 2236 mJ/cm<sup>2</sup>, at a scan speed of 1 mm/s.

that pillar growth takes place along the direction of incident of the laser beam.

4.3. Effect of mixture composition and slurry thickness

Mixtures with different compositions and thicknesses were deposited on Cu foils and irradiated. Fig. 7 shows SEM images of micro pillars formed from a Si/polyimide mixture and from Si powders only (slurry thickness 10 µm) at the same laser fluence. Distinctly different in appearance from Fig. 3(d), the micro pillars in Fig. 7 are not conical, but look like micro domes with spherical heads. This might be the result of an extensive aggregation of liquid Si due to the surface tension effect without the circumferential pressure induced by the plasma gasification and ignition of carbon black. This result demonstrates the importance of using carbon black as a sacrificial agent to achieve high aspect ratio micro pillars.

Fig. 8 plots the change in pillar height with laser fluence for different mixture compositions. As a general trend, pillar height increases with laser fluence for each mixture. The pillars generated from Si powders only are higher than those from other types of mixtures. In the case of Si powders only, liquid Si was easy to aggregate extensively due to the surface tension effect, forming big and tall pillars. In contrast, the existence of impurities and inclusions (carbon black and polyimide) did suppress the aggregation of liquid Si, leading to smaller and shorter pillars. This result demonstrates the controllability of the shape and height of micro pillars via adjusting the mixture composition and laser irradiation conditions.

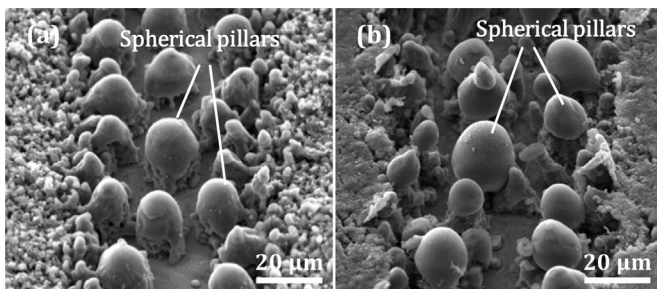


**Fig. 7.** Pillar formation for different coatings: (a) Si and polyimide, (b) Si only, at a laser influence of 2115 mJ/cm<sup>2</sup> and a scan speed of 10 mm/s.

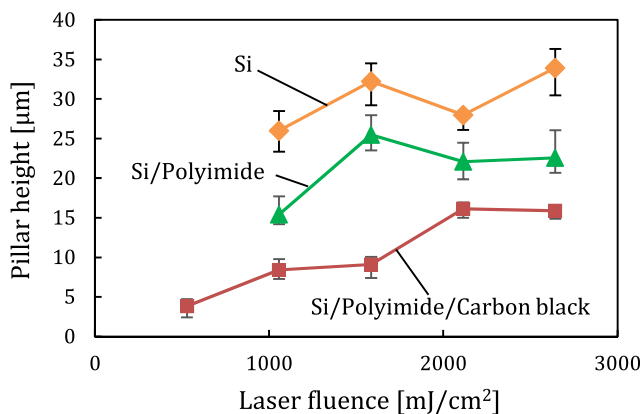


**Fig. 8.** Change of pillar height with laser fluence and composition of mixture layer.

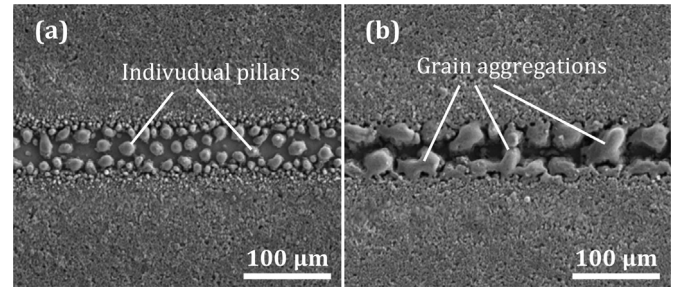


**Fig. 9.** Pillar formation at different slurry thicknesses: (a) 13 (b) 39 µm (10 mm/s, 2115 mJ/cm<sup>2</sup>).

The effect of the thickness of the slurry layer on the formation of the pillars was also investigated. It was found that a slurry layer thinner than 30 µm was suitable for generating micro pillars, which were directly bonded to the Cu foil. However, when the layer was too thick, the pillars did not bond to the Cu foil because the Si grains in the deep region were not completely melted. Fig. 9 shows top-view SEM images of laser irradiated Si/polyimide mixtures with different layer thicknesses. At a thickness of 13 µm, micro pillars were formed; while at 39 µm, Si merged into huge grains without clear pillar formation.

4.4. Cross-sectional TEM analysis of micro pillars

To examine the internal structure and crystallinity of the micro pillars, a few pillars were cut into cross-sectional samples with focused ion beam techniques and thinned to ~100 nm thick samples for transmission electron microscopy (TEM) observations. Fig. 10 presents a cross-sectional TEM image of a micro pillar formed from a mixture of Si/polyimide/carbon black at a laser fluence of 1762 mJ/cm<sup>2</sup> and a scan speed of 5 mm/s. The pillar has a homogeneous solid structure without any grain boundaries and voids. On the top of the pillar surface, an adhering layer of material with a few voids inside can be seen.

Fig. 11(a) is a 135°-rotated magnified dark-field TEM image of region A indicated in Fig. 10, where a few inclusions are seen. Fig. 11

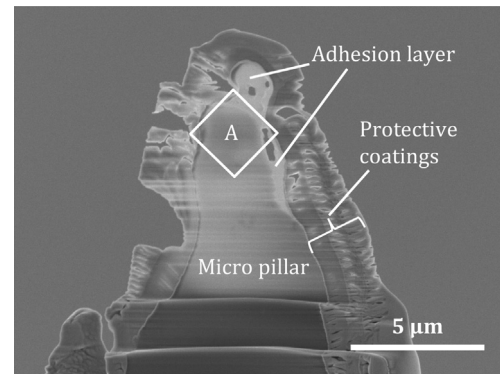


**Fig. 10.** Cross-sectional TEM sample of a micro pillar formed from a coating of Si, carbon black and polyimide at a laser fluence of 1762 mJ/cm<sup>2</sup> and a scan speed of 5 mm/s.

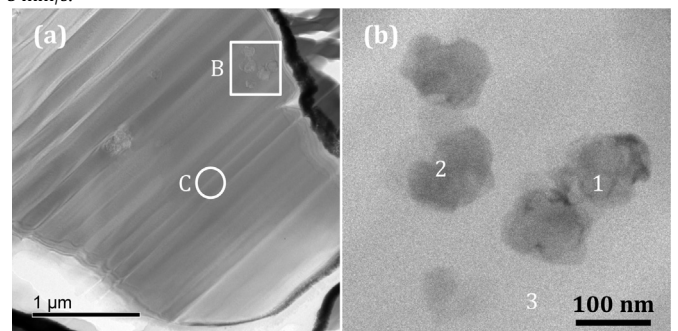


**Fig. 11.** (a) Magnified dark-field TEM image of region A indicated in Fig. 10; (b) magnified bright-field TEM image of region B in (a).

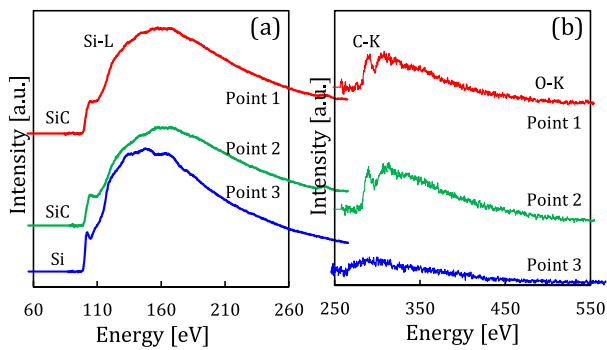


**Fig. 12.** EELS spectra of points 1–3 in Fig. 11(b). The spectra were plotted for the (a) low eV and (b) high eV regions at different vertical scales.

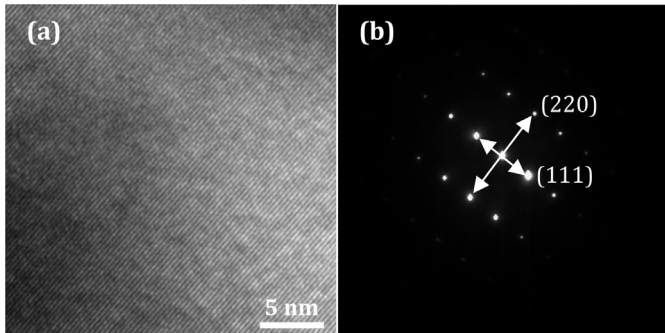


**Fig. 13.** (a) High-resolution TEM image of the crystal lattice and (b) selected-area electron diffraction pattern of region C in Fig. 11(a).

(b) is a further magnified bright-field TEM image of region B in (a). The inclusions are a cluster of particles with an average size of  $\sim 100$  nm. To further identify the chemical composition of the inclusions, electron energy loss spectroscopy (EELS) analysis was performed, and the EELS spectra of points 1–3 in Fig. 11(b) are shown in Fig. 12. The analysis shows that the inclusions are SiC grains, while the surrounding matrix is Si. EELS analysis also showed that the pillar surface was covered by a thin layer of Si oxide (thickness  $\sim 80$  nm), and that the adhering layer indicated in Fig. 10 was a mixture of Si oxide and carbon.

To examine the crystallinity of the Si matrix, high-resolution TEM observations and selected-area electron diffraction were performed. Fig. 13 shows the lattice image and diffraction pattern of area C in Fig. 11(a). Similar results were obtained for other Si matrix regions selected from all over the sample. This finding strongly demonstrates that the pillars are single-crystalline; though a small portion of carbon black is adhering to the pillar surface besides Si oxide, or embedded into the Si matrix, forming SiC inclusions. This might be a consequence of a complete melting and recrystallization of the Si powder during laser irradiation.

#### 4.5. Performance of pillar-on-foil structures as battery electrode

The fabricated pillar-on-foil structures were used as negative electrodes of lithium ion batteries, and their charge/discharge performance was evaluated. Fig. 14 illustrates the capacity change of a Si pillar electrode (Cu foil:  $40 \times 40$  mm<sup>2</sup>, mixture: Si/polyimide/carbon black, laser fluence: 1410 mJ/cm<sup>2</sup>, scan speed: 5 mm/s, line spacing: 57  $\mu$ m) with increasing number of charge/discharge cycles. For comparison, the results for a carbon electrode were also plotted. Compared with the carbon electrode, the developed Si pillar electrode improved the discharge capacity by a factor of six to ten. It is noteworthy that even though the cycle number exceeded 150, the Si pillar electrode maintained a high capacity, while the carbon electrode was significantly degraded. The long service life and stable capacity of the electrode indicate that the pillar-on-foil structure produced in this study could

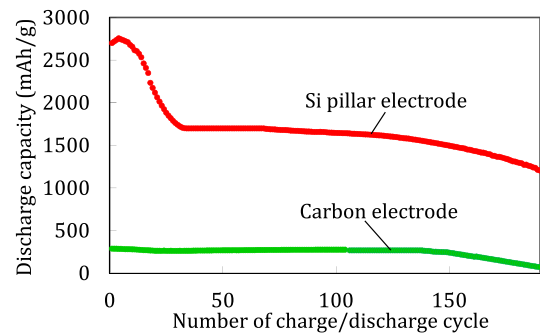


**Fig. 14.** Plots of capacity changes of a fabricated Si pillar electrode and a carbon electrode with increasing number of charge/discharge cycles.

effectively accommodate the ion storage-induced volume expansion of Si, as illustrated in Fig. 2(b). Moreover, the pillar structure increased the effective contact area between Si and the electrolytic solution, while the strong bonding between the Si pillars and the Cu foil improved the electrical conductivity of the electrode. These advantages of Si micro pillars provide the beneficial applicability of the proposed fabrication method to the manufacture of the next generation lithium ion batteries.

## 5. Conclusions

A mixture layer of waste silicon powders, polyimide, and carbon black was deposited onto a copper foil and irradiated by laser. Single-crystal silicon micro pillars with strong bonding to the copper foil were generated. The size, shape and orientation of the pillars were controllable by varying the fluence, incident angle, scan speed of the laser, as well as the composition and deposited layer thickness of the mixture slurry. The fabricated pillar-on-foil structures were used as negative electrodes for lithium-ion batteries and could effectively accommodate the volume expansion of silicon caused by ion storage. As a result, excellent discharge capacity and cycle characteristics were achieved. As a future task, the proposed fabrication process will be optimized to improve the productivity and uniformity of the micro pillars.

## References

- Atthi N, Nimittrakoolchai OU, Supothina S, Supadech J, Jearmsakiri W, Pankiew A, Hruanun C, Poyai A (2011) An Effect of Silicon Micro-/Nano-patterning Arrays on Superhydrophobic Surface. *Journal for Nanoscience and Nanotechnology* 11(10):8967–8973.
- Elbersen R, Vijselaar W, Tiggelaar RM, Gardeniers H, Huskens J (2015) Fabrication and Doping Methods for Silicon Nano- and Micropillar Arrays for Solar-cell Applications: A Review. *Advanced Materials* 27(43):6781–6796.
- Nissilä T, Sainiemi L, Sikanen T, Kotiaho T, Franssila S, Kostianen R, Ketola RA (2007) Silicon Micropillar Array Electrode Chip for Drug and Biomolecule Analysis. *Rapid Communications in Mass Spectrometry* 21(22):3677–3682.
- Jokinena V (2016) Directional Imbibition on a Chemically Patterned Silicon Micropillar Array. *Soft Matter* 12:1100–1106.
- Gowda SR, Pushparaj V, Herle S, Girishkumar G, Gordon JG, Gullapalli H, Zhan X, Ajayan PM, Reddy ALM (2012) Three-dimensionally Engineered Porous Silicon Electrodes for Li Ion Batteries. *Nano Letters* 12(12):6060–6065.
- Iwabuchi Y, Yan J (2015) Laser Sintering of Silicon Powder and Carbon Nanofibers for Porous Composite Thick Films. *Applied Physics Express* 8:026501.
- Yan J, Okada K (2016) Fabrication of Silicon-based Porous Nanocomposite Films by Focused Infrared Light Sintering. *Annals of the CIRP* 65(1):217–220.
- Li X, Gu M, Hu S, Kennard R, Yan P, Chen X, Wang C, Sailor MJ, Zhang JG, Liu J (2014) Mesoporous Silicon Sponge as an Anti-pulverization Structure for High-performance Lithium-ion Battery Anodes. *Nature Communications* 5:4105.
- Hon KKB, Gill TJ (2003) Selective Laser Sintering of SiC/Polyamide Composites. *Annals of the CIRP* 52(1):173–176.
- Deckers J, Kruth JP, Shahzad K, Vleugels J (2012) Density Improvement of Alumina Parts Produced Through Selective Laser Sintering of Alumina-polyamide Composite Powder. *Annals of the CIRP* 61(1):211–214.
- Huis in't Veld B, Overmeyer L, Schmidt M, Wegener K, Malshe A, Bartolo P (2015) Micro Additive Manufacturing Using Ultra Short Laser Pulses. *Annals of the CIRP* 64(2):701–724.
- Kruth JP, Levy G, Klocke F, Childs THC (2007) Consolidation Phenomena in Laser and Powder-bed Based Layered Manufacturing. *Annals of the CIRP* 56(2):730–759.